THREE-DIMENSIONAL FULL-DOMAIN STEADY-STATE TEMPERATURE FIELD SIMULATION ANALYSIS OF PEDAL MOTOR FOR NEW ENERGY VEHICLES

Chengcheng Zeng [1], Quanfeng Li [2]*

[1] *Shanghai DianJi University, Shanghai, China*
[2] *Shanghai DianJi University, Shanghai, China*
** liqf@sdju.edu.cn*

Keywords: PEDAL MOTORS OF NEW ENERGY VEHICLES, PERMANENT MAGNET BRUSHED DC MOTOR, SINGLE-VALUE CONDITIONS, STEADY-STATE TEMPERATURE FIELD

Abstract

Most of the pedal motors of new energy vehicles (EVPM) use permanent magnet brushed DC motors (PMDCM), which will produce additional mechanical and electrical losses during the commutation process, resulting in excessive motor temperature. This paper takes a 2-pole 12-slot EVPM as an example and establishes a three-dimensional full-domain steady-state temperature field simulation model for the motor. First, theoretical research was conducted on the loss and heat transfer mode generated by brushed DC motors during operation. Secondly, the single-value conditions required for the simulation process were analyzed and calculated. Through finite element simulation, the three-dimensional full-domain steady-state temperature field distribution law of the motor at 25℃ and a load of 0.15 mN·m was obtained. Finally, a motor temperature rise test was conducted, and the simulated values of the motor housing temperature rise were compared with the experimental values, proving the accuracy and effectiveness of the model.

1 Introduction

The PMDCM motor has the advantages of simple structure, small size, and normal operation without external control circuits [1], and is widely used in automobiles, aerospace, and other fields. The brushed motor generates additional mechanical and electrical losses during commutation, causing the motor temperature to rise excessively.

Currently, many scholars at home and abroad have conducted extensive research on the temperature field calculation of motors, mainly using equivalent thermal circuit methods and numerical calculation methods. The equivalent thermal circuit method can simplify the temperature field inside the motor into a thermal network model. S.K. Chowdlmry et al. used thermal networks to calculate and analyze the steady-state and transient temperature fields of single-phase asynchronous motors [2]. The numerical calculation method is a commonly used method in engineering for analyzing temperature fields, capable of accurately determining the temperature distribution within an electric motor. Si Jikai et al. established a finite element model of magnetic-thermal coupling and performed iterative coupling calculations on the computational results [3-5]. Literature [6-8] combines fluid dynamics with finite elements to correct the coupled equations of fluid flow and temperature field changes, thereby improving the accuracy of temperature field calculations.

The majority of domestic and international research on motor temperature field calculations has focused on the AC motors and brushless motors, with relatively little research on the temperature fields of brushed motors. This paper conducts a steady-state temperature field analysis of a 2-pole 12-slot EVPM of a certain model used in the automotive field. The single-value conditions in the temperature field simulation process were analyzed and calculated, and a three-dimensional full-domain steady-state temperature field model was established for the motor at 25°C with a load of 0.15 mN·m. The temperature distribution law of the motor under this working condition was obtained. Finally, a comparison and verification was conducted in conjunction with motor temperature rise experiments.

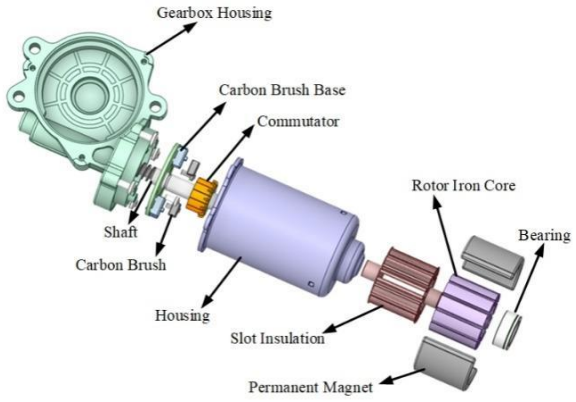

Fig. 1 The structure diagram of EVPM

2. Performance Parameters and Heat Transfer Modes of the EVPM

2.1 Main structure and performance parameters of the EVPM

This paper focuses on the temperature field analysis of a 2-pole 12-slot EVPM. The motor structure is shown in Fig 1, and the main performance parameters are shown in Table 1.

Table 1. The performance parameters of EVPM

Parameters	Unit	Value
Rated Voltage	V	12.5
Rated Speed	rpm	2300
Rated Torque	mN·m	0.15
No-load Speed	rpm	3200
Rated Current	A	4
No-load Current	A	0.8

2.2 The loss distribution of EVPM

During normal operation, due to its unique mechanical commutation structure, PMDCM generates carbon brush contact loss and friction loss between the carbon brush and commutator in addition to copper loss, iron loss, mechanical loss, and stray loss, compared to other motors [9].

The copper loss of the armature winding can be expressed by Equation (1).

$$P_{Cu} = I_1^2 R \tag{1}$$

Where: I_1 is the current when the motor is running; R is the resistance of the armature winding at the current temperature.

The rotor core loss can be divided into rotor yoke loss and tooth loss, which can be calculated using empirical formulas, as shown in Equation (2).

$$P_{Fe} = K_a P_a \left(B_t^2 G_t + B_{cj}^2 G_{cj}\right) \left(\frac{f}{50}\right)^{1.3} \tag{2}$$

Where: K_a is the iron loss correction coefficient; P_a is the iron loss per unit mass; B_t and B_{cj} are the magnetic flux density of the tooth and yoke, respectively; G_t and G_{cj} are the tooth weight and yoke weight, respectively.

Carbon brush contact wear and carbon brush friction wear with the commutator can be expressed by Equations (3) and (4), respectively.

$$P_{ds} = n I_2^2 R_{ds} \tag{3}$$

$$P_{dh} = u_{ds} F_{ds} v_1 \tag{4}$$

Where: P_{ds} is the carbon brush contact loss; I_2 is the current passing through the carbon brush when the motor is running; R_{ds} is the carbon brush contact resistance; n is the number of carbon brushes; P_{dh} is the friction loss between the carbon brush and the commutator; u_{ds} is the carbon brush friction coefficient; F_{ds} is the carbon brush pressure; v_1 is the linear speed of the rotor.

The mechanical loss of the rotor bearing can be calculated using the motor efficiency, as shown in Equation (5).

$$P_f = P_t - (P_{Cu} + P_{Fe} + P_{ds} + P_{dh}) \tag{5}$$

Where: P_f is the mechanical loss of the bearing, and P_t is the total loss of the motor.

2.3 The heat transfer method inside the motor

The various types of losses generated inside the motor are ultimately transferred in the form of heat. The main methods of transfer are heat conduction, heat convection, and heat radiation. Among these, heat conduction occurs between solids, while heat convection occurs between fluids and solids [10]. The heat conduction and heat convection can be expressed by equations (6) and (7), respectively.

$$\Phi = -\lambda A \frac{\partial t}{\partial x} \tag{6}$$

Where: Φ is the heat flux; λ is the thermal conductivity of the heat transfer surface material; A is the heat transfer area; $\partial t/\partial x$ is the rate of temperature change perpendicular to the heat transfer surface.

$$q = \alpha\left(t_w - t_f\right) \tag{7}$$

Where: q is the heat flux density; α is the convective heat transfer coefficient; t_w is the solid surface temperature; t_f is the average fluid temperature.

3 The Single-value Conditions in the Heat Transfer Process of Electric Machines

3.1 The physical conditions

3.1.1 The physical parameters: The physical parameters mainly include the density, specific heat capacity, and thermal conductivity of various materials. The physical parameters of various materials in the EVPM studied in this paper are shown in Table 2.

Table 2. The physical properties of EVPM materials

Materials	Thermal conductivity (λ)	Specific heat capacity(c)	Density (ρ)
Unit	W/(m·℃)	J/(kg·℃)	kg/m^3
Structural steel	45	448	7872
Insulating material	0.2	900	1500
Air	0.0242	1006.43	1.225
Ferrite	0.5	800	4845
Graphite	129	710	2256
Winding	400	385	8933

All materials listed in **错误!未找到引用源。** are isotropic materials. For rotor cores, they are made of laminated silicon steel sheets. During the calculation process, in order to simplify the calculation, the rotor core can be treated as an anisotropic material for overall calculation. The thermal conductivity of the equivalent rotor core in the laminated direction can be obtained from Equation (8).

$$\lambda_T = \frac{\delta_{Fe} + \delta_0}{\frac{\delta_{Fe}}{\lambda_1} + \frac{\delta_0}{\lambda_0}} = \frac{1}{\frac{K_{Fe}}{\lambda_1} + \frac{1 - K_{Fe}}{\lambda_0}} \tag{8}$$

Where: δ_{Fe} is the thickness of the silicon steel sheet; δ_0 is the thickness of the insulating varnish between the silicon steel sheets; K_{Fe} is the laminated coefficient of the core; λ_1 is the thermal conductivity of the silicon steel sheet; λ_0 is the thermal conductivity of the inter-sheet insulation.

3.1.2 The Internal Heat Source of Motor: The main sources of heat within the motor come from various types of losses generated during motor operation. This paper will apply a load to the heating element by assigning a heating power, which can be expressed by Equation (9).

$$Q = \frac{W_q}{V} \tag{9}$$

Where: W_q is the loss of the heating element inside the motor; V is the volume corresponding to the heating element.

3.2 The EVPM temperature field calculation model

3.2.1 The Basic Assumptions: Before establishing the temperature field calculation model for EVPM, the following assumptions must be made: ① The convective heat dissipation coefficient on the surface of EVPM is constant, ignoring changes in physical properties with temperature; ② The various types of losses calculated are uniformly distributed across the corresponding motor structure and are all used to generate heat and loaded into the model as heat sources; ③ The skin effect of the windings is ignored.

3.2.2 Establishment of Equivalent Calculation Models: In order to facilitate subsequent mesh partitioning and temperature field calculations, the motor model in Fig 1 needs to be simplified using SpaceClaim. When performing equivalent treatment on the slot insulation and windings, ensure that the volume of the slot insulation and windings remains unchanged after the equivalent treatment. Fig 2 shows a simplified equivalent cross-sectional view of the motor model, and Fig 3 shows an equivalent model inside the rotor slot.

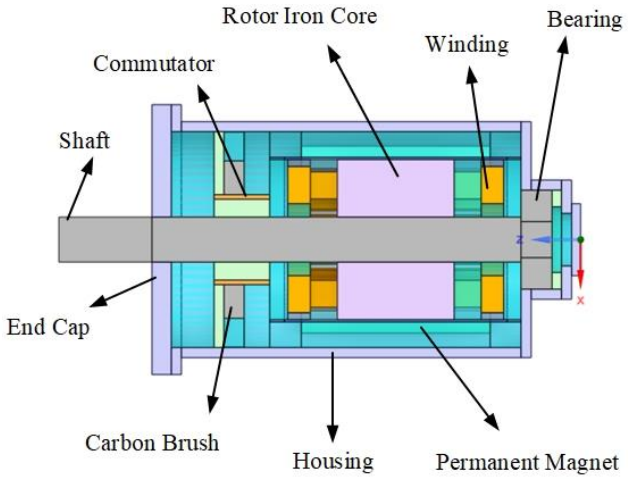

Fig. 2 Simplified equivalent cross-sectional diagram of the motor

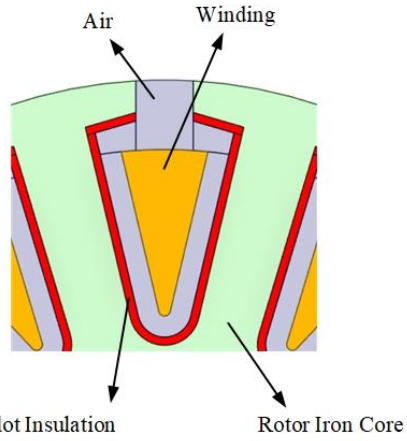

Fig. 3 Equivalent diagram of rotor slot

Fig 4 shows the air domain model inside the motor. To improve the accuracy of the simulation, the air gap of the motor needs to be named separately for subsequent rotation domain settings. The blue area within the yellow box in the figure is the air gap. The meshing of the motor and the internal air domain is shown in Fig 5.

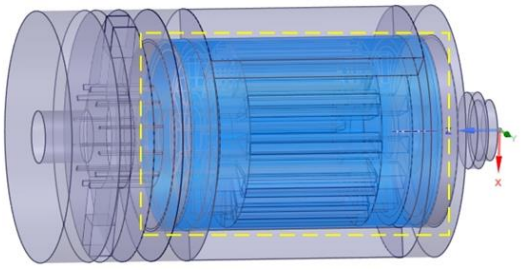

Fig. 4 Air domain model inside the motor

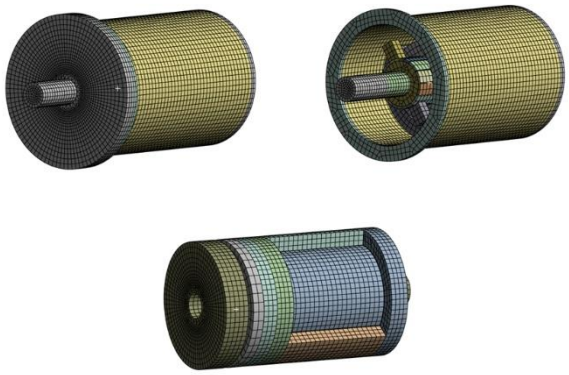

Fig. 5 The meshing of the motor and the internal air domain

This paper defines the external wall surface of the motor as a third-class boundary condition, which specifies the surface heat transfer coefficient between the object on the boundary and the surrounding fluid, as well as the temperature of the surrounding fluid. In addition, this paper mainly solves the

steady-state temperature field of the motor without considering time conditions.

4 The Steady-state Temperature Field Calculation and Analysis of EVPM

4.1 Flunet temperature field simulation calculation process

This paper will use Fluent to simulate the steady-state temperature field of EVPM at 25°C under a load of 0.15 mN·m. The main simulation process is shown in Fig 6.

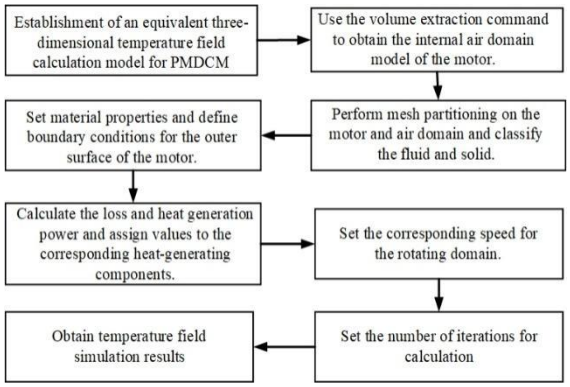

Fig. 6 The temperature field simulation process

4.2 The simulation results analysis

According to the simulation process, the steady-state temperature field of EVPM at 25°C and a load of 0.15 mN·m was simulated and analyzed, and the temperature distribution of different structures was obtained. Fig 7 and Fig 8 show the internal temperature distribution of the motor and the temperature distribution of different structures, respectively

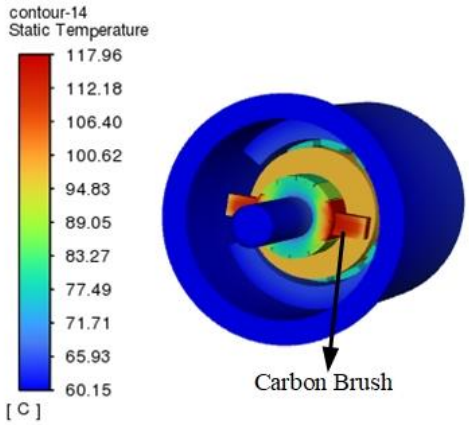

Fig. 7 The internal temperature distribution of the EVPM

As can be seen from Fig 7, after the motor temperature reaches a steady state, the carbon brushes have the highest temperature among the different motor components. As shown in Fig 8, when the motor temperature reaches steady state, the maximum temperature of the carbon brushes is 117.96°C, with a temperature rise of 92.96 K; the maximum temperature of the permanent magnets is 68.35°C, with a temperature rise of 43.35 K; the maximum temperature of the motor housing is 66.6°C, with a temperature rise of 41.6 K; and the maximum temperature of the windings is 97.8°C, with a temperature rise of 72.8 K.

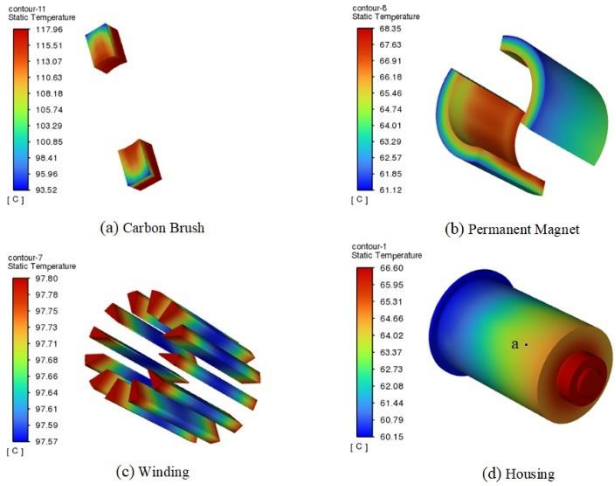

Fig. 8 The temperature distribution of different motor structures

After the motor is energized, the rotor drives the commutator to rotate, causing friction loss between the carbon brushes and the commutator. In addition, current flows through the carbon brushes, causing contact loss between the carbon brushes and the commutator due to contact resistance. Due to the small volume and low specific heat capacity of the carbon brush itself, the heat generated by loss has a significant impact on the carbon brush, causing a more obvious increase in its temperature.

There are two main ways in which windings dissipate heat to the outside environment. One is by transferring heat to the permanent magnet, motor housing, and end cover. The other is by transferring heat to the outside environment via slot insulation, rotor core, rotor shaft, bearings, and motor housing. The space around the motor rotor bearings is relatively small, and friction loss occurs when the bearings rotate. Therefore, the highest temperature in the motor housing is located at the bottom bearing area.

5 The Comparison and Analysis of Simulation Results and Experimental Results

Place the prototype in an environment of approximately 25°C and conduct a steady-state temperature rise test on the motor. The temperature rise test platform is shown in Fig 9. Fix the K-type thermocouple at point a on the surface of the housing above the permanent magnet (as shown in Fig 8). The motor is connected to the hysteresis brake via a coupling. Adjust the brake current to maintain the load at 0.15 mN·m. The temperature measuring device in the figure can be directly connected to a computer to read real-time temperature curves. The temperature rise results at point a on the surface of the machine shell are shown in Fig 10.

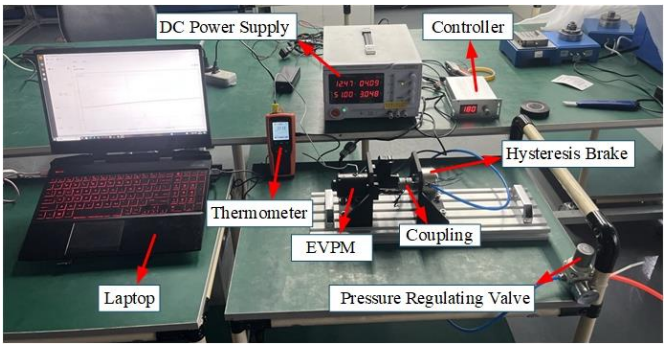

Fig. 9 The temperature rise test platform

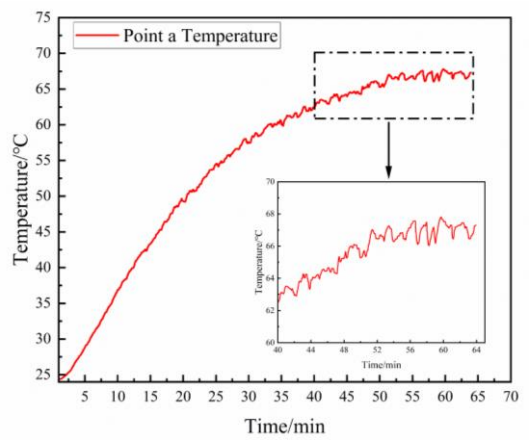

Fig. 10 The temperature rise curve at point a

As can be seen from Fig 10, after the motor has been running for 52 minutes, the temperature at point a remains around 66.63°C, indicating that the motor has reached a steady state. The results of the temperature rise experiment are compared with the previous simulation results, as shown in Table 3.

Table 3. Comparison of simulation results and experimental results for the temperature at point a on the surface of the motor housing

Operating conditions	Experimental valueT_e/K	Simulation valueT_s/K	Error/%
25°C load 0.15 mN·m	42.13	39.32	6.67%

As can be seen from Table 3, the simulation values obtained from finite element calculations are slightly lower than the experimental values. One reason for this is that when calculating motor losses, eddy current losses in permanent magnets were ignored due to the low electrical conductivity of ferrite.

6 Conclusion

This paper conducts corresponding research on the three-dimensional full-domain steady-state temperature field of EVPM. When modeling the three-dimensional temperature field, the motor model is reasonably equivalent, which improves the computational efficiency of the model. Fluent was used to calculate the steady-state temperature rise of the motor at 25°C under a load of 0.15 mN·m, and the temperature field distribution pattern of the motor under this operating condition was obtained. Finally, the actual temperature rise value at point a on the motor housing surface under this operating condition was measured through a temperature rise test and compared with the simulation results. This demonstrated that the three-dimensional full-domain steady-state temperature field model established in this paper can accurately simulate the steady-state temperature rise of this motor, providing a certain reference value for the research and optimization of the temperature rise of EVPM and PMDCM.

7 References

[1] Zhang Ji, Wang Jianchang, Liu Jiadong.: 'Modeling and prediction of electromagnetic interference in DC brush motors', Journal of Tongji University (Natural Science Edition), 2022, 50(S1), pp. 237-24

[2] S.K.Chowdhury, S.Chowdhury ,S.P. Chowdhury , S.K.Pal.: 'Performance Prediction of Single Phase Induction Motors Using Field and Thermal Models'. The Fifth International Conference on Power Electronics and Drive System, 2003, pp. 456-461

[3] Si Jikai, Zhao Suzhen, Feng Haichao, et al.: 'Analysis of temperature field for a surface-mounted and interior permanent magnet synchronous motor adopting magnetic-thermal coupling method', CES Transactions on Electrical Machines and Systems, 2018, pp. 166-174

[4] Zheng Di, Wang Dazhi, Yu Linxin, et al.: 'Electromagnetic-thermal analytical model of axial-flux permanent magnet eddy current driver', Transactions of China Electrotechnical Society, 2019, pp. 2315-2323

[5] Han Xueyan, Song Cong.: 'Research on temperature rise influencing factors and calculation of permanent magnet synchronous motor for vehicle based on magneto-thermal coupling method', Electric Machines and Control, 2020, pp.28-35

[6] Zhang Yujiao, Ruan Jiangjun, Huang Tao, et al.: 'Calculation of temperature rise in air-cooled induction motors through 3-D coupled electromagnetic fluid-dynamical and thermal finite-element analysis', IEEE Transactions on Magnetics, 2012, pp. 1047-1050

[7] Wu Baixi, Wan Zhenping, Zhang Kun, et al.: 'Design of reentrant cooling channel in permanent magnet synchronous motor considering temperature field and flow field', Transactions of China Electrotechnical Society, 2019, pp. 2306-2314

[8] Zhu Gaojia, Liu Xiaoming, Li Longnv, et al.: 'Design and analysis of the ventilation structure for a permanent magnet wind generator', Transactions of China Electrotechnical Society, 2019, pp. 946-953

[9] Chen Chen, Qian Hua, Li Zhipeng, et al.: 'Calculation and Analysis of 3D Transient Temperature Field in Brush DC Motor for Vacuum', Micro Special Motor, 2021, pp. 34-37

[10] Zhao Xiangmin.: 'Design of Cooling Structure and Temperature Field Calculation for High Power Density Oil-Cooled Flat Wire Motors Used in Vehicles'. Master thesis Harbin University of Science and Technology, 2024